Journal of General Virology (2010), **91**, 1919–1930 DOI 10.1099/vir.0.021071-0

Characterization of hepatitis C virus pseudoparticles by cryo-transmission electron microscopy using functionalized magnetic nanobeads

Pierre Bonnafous,[1]† Marie Perrault,[2]† Olivier Le Bihan,[1] Birke Bartosch,[3,4,5]‡ Dimitri Lavillette,[3,4,5] François Penin,[2] Olivier Lambert[1]† and Eve-Isabelle Pécheur[2]†

Correspondence
Olivier Lambert
o.lambert@cbmn.u-bordeaux.fr
Eve-Isabelle Pécheur
e.pecheur@ibcp.fr

[1]CBMN, UMR CNRS 5248, Université Bordeaux 1, ENITAB, IECB, Avenue des Facultés, F-33405 Talence, France

[2]Institut de Biologie et Chimie des Protéines, UMR CNRS 5086, Université Lyon 1, IFR128 Lyon Biosciences Gerland, F-69007 Lyon, France

[3]Université de Lyon, UCB-Lyon 1, IFR128, F-69007 Lyon, France

[4]INSERM, U758, F-69007 Lyon, France

[5]Ecole Normale Supérieure de Lyon, F-69007 Lyon, France

Cell entry and membrane fusion of the hepatitis C virus (HCV) depend on its envelope glycoproteins E1 and E2. HCV pseudotyped particles (HCVpps) are relevant and popular models to study the early steps of the HCV life cycle. However, no structural characterization of HCVpp has been available so far. Using cryo-transmission electron microscopy (cryo-TEM), providing structural information at nanometric resolution, the molecular details of HCVpps and their fusion with liposomes were studied. Cryo-TEM revealed HCVpps as regular 100 nm spherical structures containing the dense retroviral nucleocapsid surrounded by a lipid bilayer. E1–E2 glycoproteins were not readily visible on the membrane surface. Pseudoparticles bearing the E1–E2 glycoproteins of Semliki forest virus looked similar, whereas avian influenza A virus (fowl plague virus) haemagglutinin/neuraminidase-pseudotyped particles exhibited surface spikes. To further characterize HCVpp structurally, a novel method was designed based on magnetic beads covered with anti-HCV antibodies to enrich the samples with particles containing E1–E2. This strategy efficiently sorted HCVpps, which were then directly observed by cryo-TEM in the presence or absence of liposomes at low or neutral pH. After acidification, HCVpps looked the same as at neutral pH and closely contacted the liposomes. These are the first visualizations of early HCV membrane fusion events at the nanometer scale. Furthermore, fluorimetry analysis revealed a relative resistance of HCVpps regarding their fusion capacity when exposed to low pH. This study therefore brings several new molecular details to HCVpp characterization and this efficient strategy of virion immunosorting with magnetic nanobeads is direct, efficient and adaptable to extensive characterization of any virus at a nanometric resolution.

Received 18 February 2010
Accepted 6 April 2010

INTRODUCTION

Hepatitis C virus (HCV) is a major cause of chronic hepatitis, cirrhosis and hepatocellular carcinoma. HCV belongs to the genus *Hepacivirus* of the family *Flaviviridae* (Lindenbach & Rice, 2001). The two surface proteins, E1 (aa 192–383) and E2 (aa 384–746), are processed by signal peptidases of the endoplasmic reticulum from a 3000 aa polyprotein encoded by the HCV positive-sense RNA genome (reviewed by Moradpour *et al.*, 2007). The E1 (approx. 31 kDa) and E2 (approx. 70 kDa) proteins are glycosylated in their large N-terminal ectodomains (Helle *et al.*, 2007) and anchored into the membrane by their C-terminal transmembrane domains. E1 and E2 form a heterodimer, which is thought to be the pre-budding form

†These authors contributed equally to this work.

‡Present address: INSERM, U871, F-69003 Lyon, France; Université Lyon 1, IFR62 Lyon-Est, F-69008 Lyon, France; Hospices Civils de Lyon, Hôtel Dieu, Service d'hépatologie et de gastroentérologie, F-69002 Lyon, France.

of the functional complex (Op De Beeck *et al.*, 2001), present at the surface of HCV particles (Op De Beeck *et al.*, 2004) and is involved in virus entry. HCV E2 is responsible for virion attachment to target cells and can bind different receptors including capture molecules such as glycosaminoglycans, the CD81 tetraspanin and the scavenger receptor BI (reviewed by Bartosch & Cosset, 2006; Helle & Dubuisson, 2008). The role of E1 in HCV infection remains unclear; however, antibodies directed against E1 are able to neutralize cell entry, presumably at a stage distinct from receptor binding (Dreux *et al.*, 2006; Keck *et al.*, 2004). Both E1 and E2 have been reported to contain fusion determinants or fusion peptide candidates, suggesting that distinct regions in both E1 and E2 may cooperate to drive the fusion process to completion (Lavillette *et al.*, 2007). A recent study by Krey *et al.* (2010) proposed a model of the E2 ectodomain, based on disulfide connectivities, functional data and secondary-structure predictions. The tertiary organization in three domains threads E2 onto a class II fusion protein template and highlights a fusion loop candidate. This model has revealed large, poorly structured regions of the E2 ectodomain.

However, little is known about the molecular events that mediate HCV membrane fusion. Significant progress has been made possible with the development of HCV pseudoparticles (HCVpps), consisting of unmodified HCV E1–E2 glycoproteins assembled onto retrovirus core particles (Bartosch & Cosset, 2009; Bartosch *et al.*, 2003a; Drummer *et al.*, 2003; Hsu *et al.*, 2003), and with the isolation of an infectious HCV clone able to replicate and produce virus particles in cell culture (HCVcc) (Lindenbach *et al.*, 2005; Wakita *et al.*, 2005; Zhong *et al.*, 2005). HCVpps are a most convenient surrogate model for HCV, as they can be handled in a Biosafety Level 2 laboratory and their extensive characterization has shown that they closely mimic the early steps of HCV entry (Bartosch & Cosset, 2006; Helle & Dubuisson, 2008). However, no structural characterization of HCVpps has been available so far.

Infection assays and our *in vitro* liposome fusion assay have established that HCV entry and fusion are pH dependent (Bartosch *et al.*, 2003b; Hsu *et al.*, 2003; Lavillette *et al.*, 2006). This has been confirmed in cell–cell fusion assays (Kobayashi *et al.*, 2006) and with HCVcc (Blanchard *et al.*, 2006; Haid *et al.*, 2009; Koutsoudakis *et al.*, 2006; Tscherne *et al.*, 2006). These studies suggested that HCV cell entry occurs by endocytosis; the low endosomal pH could then promote rearrangement of the fusion protein to its functional and active form. Although the morphology of HCV is beginning to be unravelled (Wakita *et al.*, 2005; Yu *et al.*, 2007), and biochemical evidence suggests that HCV-mediated fusion is triggered at low pH, the actual HCV membrane fusion steps have not yet been visualized.

In this study, we therefore aimed to characterize the molecular details of HCVpps and HCV-mediated fusion through direct visualization of this process on a nanometric scale by cryo-transmission electron microscopy (cryo-TEM). This cryo-TEM method (Dubochet *et al.*, 1988) consists of the vitrification of aqueous suspensions (virus, liposomes, nanoparticles, etc.) into liquid ethane. Rapid freezing followed by observation of the frozen hydrated samples prevents notorious artefacts induced during sample preparation for conventional electron microscopy (such as chemical fixation, heavy-metal staining and dehydration procedures) and allows direct sample observation in a native hydrated state close to solution conditions. Consequently, cryo-TEM allows direct visualization of molecular architecture at subnanometer resolutions using subsequent three-dimensional image analysis. Using cryo-TEM, we visualized HCVpps exposed to neutral or low pH. For further characterization, magnetic nanotools were developed in order to: (i) sort relevant virus particles in terms of the presence of envelope HCV glycoproteins at their surface; and (ii) visualize membrane fusion events between pseudotyped particles and liposomes under low-pH conditions.

RESULTS AND DISCUSSION

Morphology of pseudotyped particles

Pseudoparticles are composed of a retroviral nucleocapsid surrounded by a lipid bilayer anchoring envelope glycoproteins as shown in Fig. 1 (central diagram). Three types of pseudoparticle were produced that contained the glycoproteins of HCV (HCVpps), Semliki forest virus (SFVpps) and avian influenza A virus [haemagglutinin (HA) and neuraminidase (NA); AIVpps]. A fourth construction devoid of any viral glycoprotein (NoEnvpps) was also prepared. These four pseudotyped particles were all checked for their fusion capacity by fluorimetry, as described previously (Lavillette *et al.*, 2006). They were visualized by cryo-TEM, which allowed the preservation of their native form (Fig. 1). All pseudoparticles exhibited a spherical and regular shape, with a mean diameter of 110–115 nm. For each particle, the 4 nm lipid bilayer (Fig. 1, black arrow) and the 70–80 nm faceted retroviral capsid (Fig. 1, asterisk) could readily be observed. Occasionally, pseudoparticles contained more than one retroviral capsid (data not shown). The HCVpp surface (Fig. 1a) appeared smooth, displaying no obvious protrusions and resembled NoEnvpps (Fig. 1b). However, HCV E1 and E2 were indeed present on the surface of HCVpps, as revealed by an immunogold-labelling approach (Fig. 1a, arrowheads in left panels), whereas NoEnvpps used as controls appeared devoid of any gold particles under the same conditions (Fig. 1b, upper left panel).

In order to determine whether this smooth and spikeless appearance was specific to HCVpps and/or to the nature of their envelope glycoproteins, we observed SFVpps (Fig. 1c) and AIVpps (Fig. 1d) as prototypes for particles bearing envelope proteins lying flat on the surface of the virus (SFV E1 and E2) and protruding from the bilayer (AIV HA and

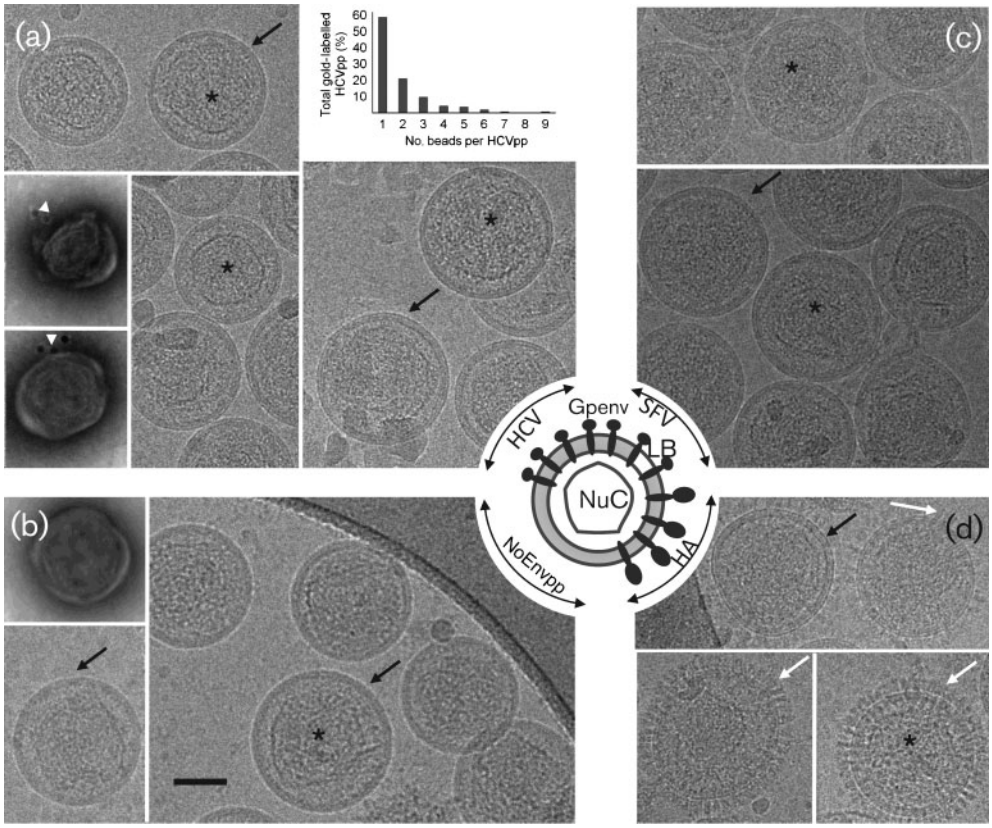

Fig. 1. Morphology of pseudoparticles observed by EM. The central diagram of pseudotyped particles depicts the constitutive elements: nucleocapsid (NuC), lipid bilayer (LB) and envelope glycoproteins (Gpenv), i.e. E1–E2 from HCV, E1–E2 from SFV, haemagglutinin (HA) and neuraminidase (NA) from AIV. NoEnvpp is a construct without Gpenv. (a–d) HCVpp (a), NoEnvpps (b), SFVpps (c) and AIVpps (d) were observed by cryo-TEM. Nucleocapsids (asterisks) and lipid bilayers (black arrows) are clearly visible. HA and NA spikes protrude from the AIVpp surface [white arrows in (d)]. The structures were also observed by conventional TEM after immunolabelling and negative staining [lower left panels of (a) and upper left panel of (b)]. HCVpps were reacted with antibodies against E1 (mAb A4, top panel) or E2 (mAb H53, bottom panel), followed by immunogold labelling, fixation and negative staining (see Methods). NoEnvpps were reacted with mAb H53 but no immunolabelling was detected [upper left panel of (b)]. The upper right graph in (a) is a histogram summarizing the distribution of gold beads on H53-labelled HCVpp (see text for details).

NA), respectively (Fujiyoshi *et al.*, 1994; Harris *et al.*, 2006). The SFVpp images did not reveal any additional protein density surrounding the outer leaflet of the lipid bilayer, although the envelope glycoproteins are reported to extend approximately 4–5 nm from the membrane (Mancini *et al.*, 2000; Paredes *et al.*, 1993), and despite immunogold labelling approaches revealing the presence of the E1 glycoprotein of SFV at the surface of SFVpps (data not shown). One plausible explanation is that the overall number of E1–E2 SFV complexes per particle was low and was therefore insufficient to provide enough contrast for their direct observation. Together with the reported flat arrangement of the E1–E2 SFV proteins on the viral membrane, low protein density at the particle surface may explain our difficulty in visualizing SFVpp proteins. This could also be valid in the context of HCVpps. SFV belongs to the family *Togaviridae*, phylogenetically close to the family *Flaviviridae* and originating from a common ancestor; it therefore constitutes a relevant model as a class II viral fusion protein for our control experiments. Nevertheless, we must keep in mind that some architectural dissimilarities are discernible between members of the *Togaviridae* and *Flaviviridae* (reviewed by Kielian, 2006; Mukhopadhyay *et al.*, 2005; Strauss & Strauss, 2001). As HCV belongs to the *Flaviviridae*, it might share morphological and structural characteristics with other viruses of this family. Indeed, both dengue and West Nile viruses display a smooth particle surface, showing no membrane projection or spike (Mukhopadhyay *et al.*, 2003; Zhang *et al.*, 2003). Likewise, Yu *et al.* (2007) described the HCV virion produced from cultured cells (HCVcc) as a particle with a spikeless outer membrane, despite some HCVcc heterogeneity having been reported by others (Lindenbach *et al.*, 2005).

From both negative-staining TEM (data not shown) and cryo-TEM observations, AIVpps clearly exhibited approximately 13 nm long spikes protruding from the lipid membrane with a radial orientation (Fig. 1d, white arrows), corresponding to the HA and NA molecules. This observation agrees well with recent cryo-electron tomography analyses, reporting a height of 14 nm for HA and 16 nm for NA (Harris *et al.*, 2006), in agreement with sizes reported for other class I fusion proteins (see, for example, Zhu *et al.*, 2006). Among AIVpps, we observed particles with high and low spike densities and even 'bald' particles, reflecting variability in the numbers of glycoprotein molecules at the particle surface. Such variability probably also affected SFVpps and HCVpps, and seems inherent to the pseudoparticle production process. Indeed, the amount of viral glycoprotein per particle depends, to a large extent, on protein expression, intracellular localization and incorporation during particle assembly and budding. It is possible that, for reasons of differential co-localization of HA and NA compared with HCV E1–E2 with the retroviral nucleocapsid, the incorporation of some glycoproteins (e.g. HA/NA) would be a more efficient process than that of others (e.g. HCV E1–E2 or flavivirus glycoproteins) (Sandrin & Cosset, 2006). This would be in agreement with the corresponding virus titres obtained for each pseudoparticle type, routinely around 10^8 international units (IU) ml^{-1} for AIVpp, but only 10^6 IU ml^{-1} for HCVpps and SFVpps.

In order to characterize HCVpps further with respect to these features, we performed analysis of the number of gold beads present at the surface of HCVpps, using monoclonal antibody (mAb) H53-immunolabelled samples deposited on the grids that were prepared for TEM observations (see Fig. 1a). We counted 450 HCVpps in total, and of these 40 % were found to be labelled with at least one gold bead. We then counted more specifically the frequency of the presence of one or more gold beads per particle. Our results are presented in Fig. 1a (graph). Of the 40 % of HCVpps labelled with gold beads, we found that ~60 % displayed one gold bead, 20 % two, 10 % three and ~5 % four gold beads. Performing similar counts with NoEnvpps resulted in zero particles labelled with gold beads.

These data clearly indicated that HCVpps are positive for E1–E2 protein complexes and that a high number of HCVpps expose several complexes available for antibody recognition. However, it must be kept in mind that these counts cannot be considered an exact quantification of a given condition in a given sample, for two reasons: (i) HCVpps are randomly distributed on the grid surface, exposing or not the epitopes of their envelope glycoproteins to the antibody; and (ii) it is well known that, in a sample of gold-labelled secondary antibody, only a limited number of antibody molecules is labelled. Overall, this might contribute to an underestimation of the number of protein complexes present at the surface of the HCVpps.

Taken together, these data point to the presence of several E1–E2 complexes at the surface of HCVpps, but these complexes could not be revealed by cryo-TEM observation. It might therefore be possible that their structure and/or global arrangement on the pseudoparticle membrane did not allow their visualization by TEM, even by high-resolution cryo-TEM.

HCVpp characterization using magnetic nanobeads

As only 40 % of HCVpps were positive for E1–E2, we wanted to enrich our samples with particles harbouring E1–E2 at their surface. For this purpose, we designed a method based on the use of 200–300 nm magnetic beads to facilitate an immunosorting strategy, followed by direct observation by cryo-TEM (Fig. 2). Superparamagnetic nanobeads (Bio-Adembeads) covered with a hydrophilic polymer conjugated to protein A or protein G (Fig. 2a, inset) were incubated with mAb H48 or H53 directed against conformation-dependent epitopes of E2 (Op De Beeck *et al.*, 2004). Excess mAbs were easily removed by magnetic concentration of the Bio-Adembeads and washing of the pellet with buffer. HCVpps were added to the mAb– protein A–bead complexes. A second purification step with a magnet eliminated HCVpps that had not bound to the bead surface. We checked that, in the absence of mAb, HCVpps did not interact with magnetic beads in a non-specific manner (Fig. 2a). Cryo-TEM observations of HCVpp immunopurified with mAbs H48 and H53 revealed HCVpps attached to Bio-Adembeads (Fig. 2b, c), whereas a similar procedure did not lead to any 'trapping' of NoEnvpp (data not shown). HCVpps could also be immunopurified using the anti-HCV E1 mAb A4, whilst NoEnvpps were again not retained by this antibody (data not shown). This indicated that our strategy relied on the specific recognition of the A4 epitope on E1 or H48 and H53 epitopes on E2. Very similar results were obtained using protein G-coated magnetic beads (data not shown). HCVpps looked similar to those observed in Fig. 1(a). HCVpps not trapped on the beads also looked similar to those attached to the beads (data not shown). This demonstrated that the mAb-sorted particles displayed a similar morphology to those not retained on the beads. Again, and despite the E1 or E2 immune-specific purification of HCVpps, we did not observe the E1–E2 glycoprotein complex at the lipid surface.

Although these results provided evidence that bound pseudoparticles do expose E1–E2 glycoproteins, their density possibly hindered their direct visualization by cryo-TEM. Interestingly, a model of the E2 ectodomain based on disulfide connectivities, functional data and secondary-structure predictions has been recently proposed by Krey *et al.* (2010). This model revealed large, poorly structured parts of the E2 ectodomain. Moreover, by analogy to flavirirus E glycoprotein, HCV glycoproteins might be flat at the viral envelope surface, and both E1 and E2 are small proteins. Finally, the high degree of glycosylation of E1 and E2 probably creates a hydrophilic

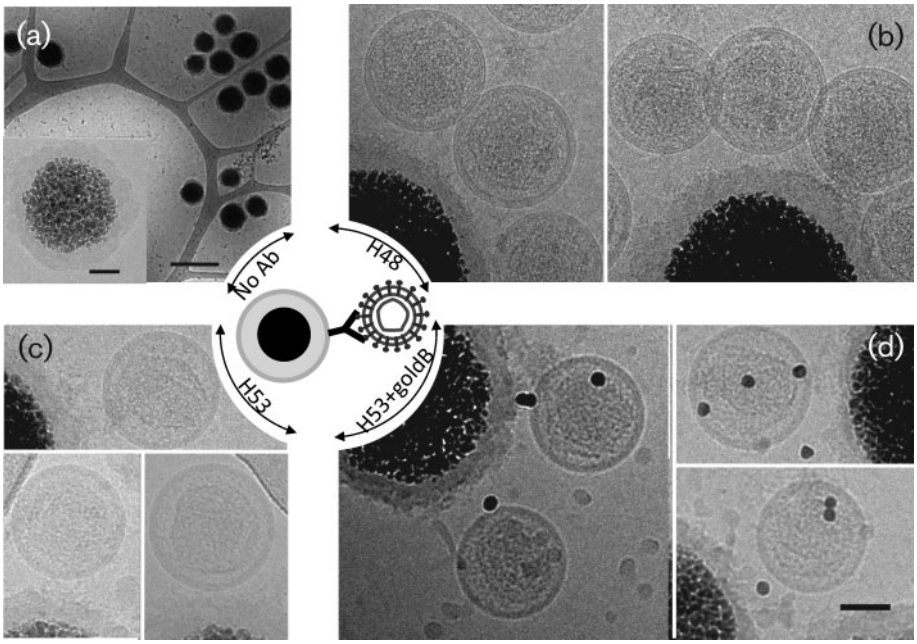

Fig. 2. Cryo-TEM visualization of HCVpps containing E2 sorted with protein A–magnetic nanobeads at neutral pH. Immunosorting of HCVpps was carried out with H48 or H53 anti-HCV E2 mAb. (a) Protein A-coated magnetic beads do not interact with HCVpps in the absence of mAbs. Bar, 50 nm. Inset, high magnification of a magnetic nanobead surrounded by a protein A-grafted polymer cushion producing a lower contrast. Bar, 1 μm. (b, c) HCVpps were immunosorted and readily observed around magnetic beads coated with mAb H48 (b) or H53 (c), respectively. (d) From the sample shown in (c), HCVpps were immunolabelled directly with H53 and detected by cryo-TEM using protein A conjugated to 10 nm colloidal gold. Bar, 50 nm.

layer at the surface of the particle. Altogether, these data could render the direct TEM observation of E1–E2 difficult, if not impossible.

The double advantage of these magnetic beads is therefore that: (i) the use of an anti-E1 or anti-E2 mAb allows specific sorting of HCVpps containing E1 or E2; and (ii) HCVpps bound to magnetic beads can be observed directly by cryo-TEM without any further treatment. Although we could not provide exact quantitative data on the number of particles trapped by the magnetic beads, the number of HCVpps observed on the TEM grid after sorting was reproducibly less than before sorting, and the Bio-Adembeads were not saturated by E2 attachment.

To evaluate whether additional E1–E2 complexes were accessible on immunopurified HCVpps, HCVpp immunolabelling was carried out on HCVpps attached to the magnetic beads. mAb H53 was mixed with sorted HCVpps and excess mAb was removed using the magnet procedure. Protein A-coupled 10 nm gold beads were added as a marker (see Methods for details). After separating out labelled HCVpps with the magnet, a few gold beads were observed in contact with HCVpps, revealing the presence of E2 and most probably of E1–E2 complexes (Fig. 2d). Altogether, these results confirmed that E2, most probably in a complex with E1, is present on the surface of HCVpps, as shown by TEM in the context of HCVpps (Chapel *et al.*, 2007) and HCVcc (Wakita *et al.*, 2005). This also clearly indicated that some E2 glycoproteins are still free for further interaction, based on our sorting procedure for HCVpps with anti-E2 mAb–protein A/G–gold bead complexes. Moreover, it demonstrated that these E2 glycoproteins exposed their epitope correctly, which is a clear indication that these molecules are functional, even though they could not be visualized directly. This again is consistent with the idea that HCV envelope glycoproteins share structural features with those of other viruses of the family *Flaviviridae* (see above) (Krey *et al.*, 2010; Mukhopadhyay *et al.*, 2003; Zhang *et al.*, 2003).

To investigate this point further, we performed Western blotting analyses before and after immunocapture of HCVpps onto H48-coated magnetic beads, to evaluate the number of captured particles. Particles were then retrieved and analysed for the presence of the murine leukemia virus (MLV) capsid and HCV E1 and E2 proteins. As presented in Fig. 3, both HCV E1 and E2 were clearly visible after sorting (compare lanes 1 and 2 for HCVpps). In order to obtain a comparable signal on the photographic film before and after sorting, we concentrated the sorted virus particles 25-fold compared with the stock HCVpps. NoEnvpps were not retained on the beads by this procedure in accordance with the fact that they are devoid

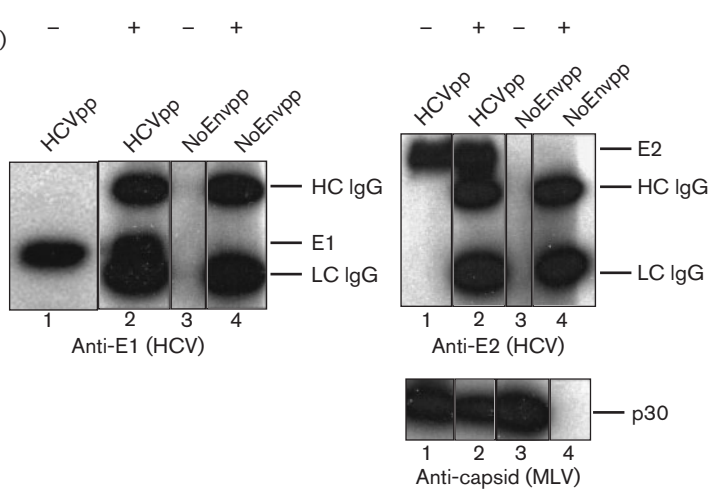

Fig. 3. Western blot analysis of particles immunosorted using magnetic beads. HCVpps and NoEnvpps were incubated with anti-E2 H48 mAb and mixed with protein G-coated magnetic beads. After 1 h on ice, the mixture was deposited onto a magnetic column and washed extensively, and the immunosorted material was released by adding boiling Laëmmli buffer. After SDS-PAGE separation, Western blotting was performed using antibodies directed against the MLV capsid (anti-p30), HCV E1 (A4) or HCV E2 (H52). Lanes 1 and 3, stock suspensions of HCVpps or NoEnvpps; lanes 2 and 4, HCVpps or NoEnvpps after immunosorting and 25-fold concentration. HC, Heavy chain; LC, light chain.

of any envelope protein. This demonstrated that our immune-sorting procedure was specific for HCV envelope proteins. A similar sorting procedure was applied to SFVpps and AIVpps leading to the enrichment of pseudoparticles containing SFV and AIV glycoproteins (data not shown).

This immune-sorting strategy was also successfully applied to AIVpps using magnetic beads coated with a polyclonal antibody directed against the H7 subtype of HA. The results presented in Fig. 4 clearly showed several AIVpps attached to antibody-coated beads at low magnification (Fig. 4a, arrows) and at higher magnification pseudotyped particles harbouring HA and NA spikes at their surface (Fig. 4b, c). This procedure was also carried out on SFVpps using a rabbit polyclonal anti-E1 serum (data not shown). SFVpps were successfully trapped around magnetic beads at neutral pH and had a morphology similar to that described in Fig. 1(c) (data not shown). In particular, no glycoprotein was visible, suggesting again, as for HCVpps, that only a small number of glycoproteins, possibly lying flat, might be present at the virus surface.

We therefore clearly demonstrated that the use of magnetic nanobeads can be extended to pseudoparticles other than HCVpps and potentially to virtually any virus, provided that an antibody is available. This strategy thus emerges as an efficient and direct approach for the structural and morphological characterization of viruses, particularly when only low-titre virus samples are available.

HCVpp characterization at low pH by cryo-TEM

As HCV entry was shown to be pH dependent, we wanted to study HCVpp morphology and behaviour at low pH. Recently, Lavillette *et al.* (2006) showed, using fluorescence spectroscopy, that HCVpps interact and exhibit a full fusion process with liposomes at low pH. We therefore wanted to observe HCVpps mixed with liposomes under similar conditions. We first noticed that HCVpps were not in contact with liposomes at neutral pH (data not shown), which was consistent with the notion that fusion does not occur at pH 7.4 (Lavillette *et al.*, 2006). We then observed a comparable morphology of HCVpps at low pH in the presence of liposomes and at neutral pH in the absence of liposomes (Fig. 5a compared with Fig. 1a). In addition, liposomes were seen in close contact with HCVpps. As the leaflets of the viral and liposomal membranes at the contact point remained well resolved, this suggested that this attachment did not extensively perturb the membranes. To assess whether liposomes interacted with HCVpps bearing E1–E2 glycoproteins, we then investigated liposome interactions with HCVpps immunosorted with mAb H53. First, we confirmed that HCVpps could be visualized at low pH using protein A/H53-coated Bio-Adembeads. For this, HCVpps were immunosorted at neutral pH. The pellet was then resuspended in buffer at pH 5.0. HCVpps remained well trapped by the magnetic beads in this low-pH context (Fig. 5b, c), and displayed features similar to those observed in Figs 1(a) and 5(a).

This already suggested a certain resistance of HCVpps to low pH (see below). Notably, mAb H48 was reproducibly less efficient at retaining HCVpps after low-pH application (data not shown), suggesting either that the interaction between H48 and HCV E2 was labile at low pH or that the H48 conformation-dependent epitope in E2 was not exposed properly at low pH, or a combination of both. Interestingly, Op De Beeck *et al.* (2004) reported a reduced E2 signal towards most antibodies including H48 after low-pH treatment of HCVpps, whereas no alteration was observed in the case of H53. These results thus suggest either a decrease at low pH of the affinity of the antibody for its epitope or a pH-dependent conformational change involving the H48 epitope on E2, which is then not well exposed, or both.

Secondly, we added liposomes to HCVpp–H53–bead complexes at neutral pH and lowered the pH. Cryo-TEM

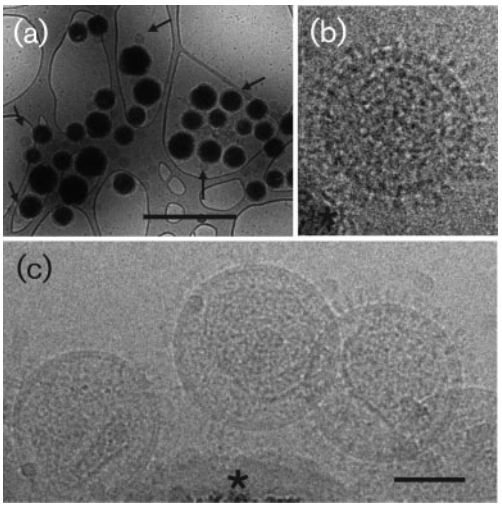

Fig. 4. Cryo-TEM visualization of AIVpps sorted by protein A–magnetic nanobeads at neutral pH. Immunosorting of AIVpps was carried out with a polyclonal antibody directed against the H7 HA subtype. (a) At low magnification, AIVpps are concentrated around the protein A-coated magnetic beads (arrows). Bar, 1 μm. (b, c) At higher magnification, AIVpps exhibiting spikes were in close contact with magnetic beads (asterisks). Bar, 50 nm.

images suggested that liposomes attached to E2-immunopurified HCVpps at low pH (Fig. 5d, e). HCV envelope glycoproteins probably played a major role in this attachment step, as NoEnvpps were not observed in contact with liposomes at any pH (data not shown). No HCVpp interaction with liposomes was observed at neutral pH (data not shown), indicating that the low pH played a role. The number of liposomes bound to HCVpps did not increase when an excess of liposomes was added.

To characterize the HCVpp–liposome interaction further, we designed another experimental set-up in order to maintain all E1–E2 complexes available for liposome interactions at low pH. As shown in Fig. 6(a), streptavidin-coated magnetic beads were incubated with liposomes containing *N*-biotinylated dipalmitoyl phosphatidylethanolamine (biotin–PE). After washing of unbound liposomes, HCVpp were added and observation by cryo-TEM was performed after extensive washing. Liposomes were observed in the vicinity of the beads (Fig. 6b, c) and HCVpps in the vicinity of liposomes (Fig. 6d–g). This is the first visualization of an essential early step in HCV fusion mediated by its envelope glycoproteins, namely the phase where these proteins closely contact the target membrane in order to initiate the actual fusion process. By analogy to related viruses of the families *Flaviviridae* and *Togaviridae* (reviewed by Kielian, 2006), conformational rearrangements in the E1–E2 fusion complex of HCV could be hypothesized, occurring in a low-pH environment in order to attract viral and liposomal membranes in the closest apposition to bring about fusion. Together with our

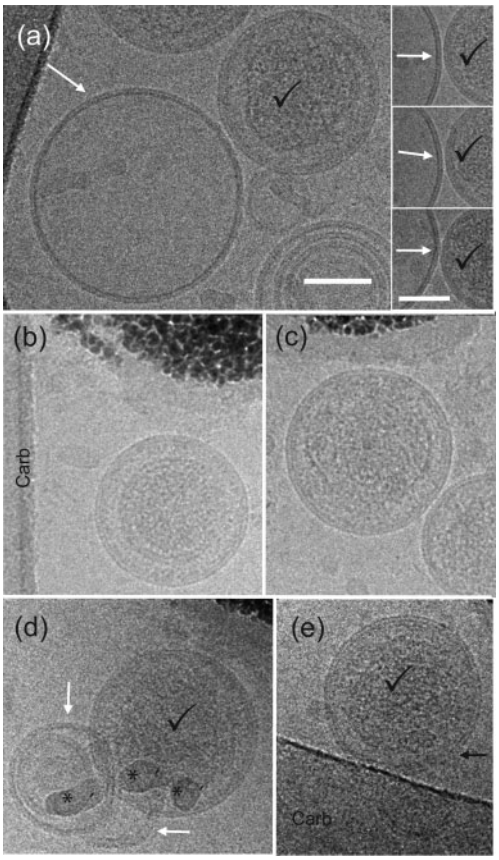

Fig. 5. Interactions between HCVpps and liposomes at low pH, using HCVpp capture. (a) Cryo-TEM observations of HCVpps (ticks) in close contact with liposomes (white arrows) after mixing at pH 5.0. Right panels, gallery of contact events. At neutral pH, no interaction between HCVpps and liposomes was encountered (not shown). (b, c) HCVpps immunosorted with H53 at low pH. (d, e) Liposomes and HCVpps immunosorted with H53 were mixed at neutral pH before lowering the pH to 5.0, followed by a purification step at pH 5.0. The black and white arrows indicates the liposome in contact with HCVpp. Asterisks, ice contaminants; Carb, carbon film. Bars, 50 nm.

observation that HCVpps can be captured on magnetic beads at low pH with mAb H53 but not with mAb H48, this lends further support to the hypothesis that the E1–E2 complex is dissociated at low pH (Op De Beeck *et al.*, 2004), leading to the exposure of fusion determinant(s) (Lavillette *et al.*, 2007). The direct visualization of later fusion events was difficult, despite our efforts, most probably because the absolute number of fusion events is low and therefore the probability of seeing them under the microscope is also low.

HCVpp fusion behaviour at low pH by fluorimetry

We next aimed to dissect the effect of low pH on HCVpp fusion behaviour to gain further information on the HCV

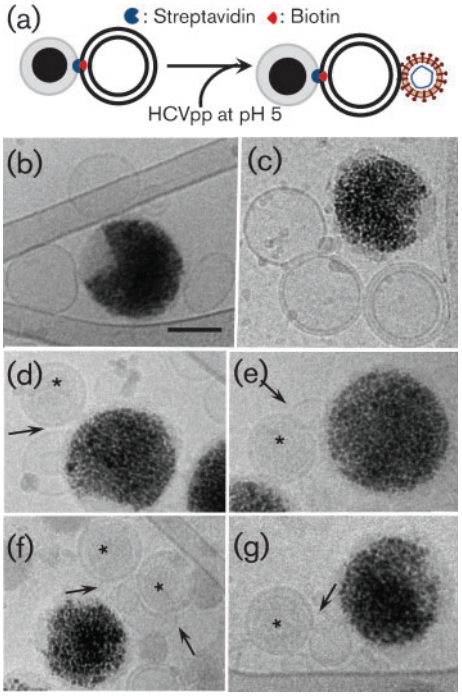

Fig. 6. Interactions between HCVpps and liposomes at low pH, using liposome capture. (a) LUVs containing biotin–PE were attached to streptavidin-coated magnetic beads. HCVpps were then captured via liposome interactions at low pH, as shown schematically. (b, c) Magnetic beads closely surrounded by liposomes at pH 7.4 and 5, respectively. (d–g) HCVpps (asterisks) interacting with liposomes attached to beads. Arrows indicate contacts between HCVpps and liposomes. Bar, 100 nm.

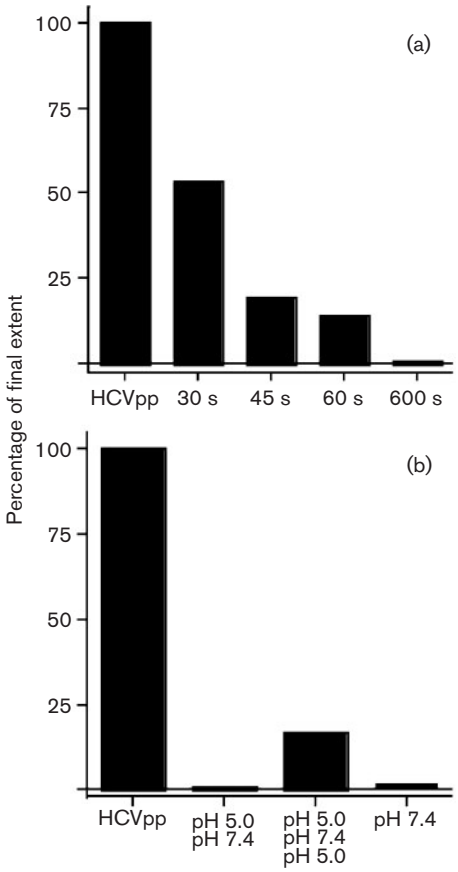

Fig. 7. Fusion behaviour of HCVpps exposed to low pH. (a) HCVpps were pre-incubated at pH 5.0 in the absence of liposomes for the indicated times. Liposomes were then added and lipid mixing was recorded by fluorimetry (see Methods for details). The results are expressed as a percentage of the final extent of fusion, taking the HCVpp–liposome fusion without any low pH pre-incubation as 100 %. (b) HCVpps were pre-incubated at pH 5.0 for 1 min in the absence of liposomes and the pH was returned to pH 7.4 by adding an appropriate volume of 1 M NaOH. Liposomes were added and lipid mixing was recorded (pH 5.0/pH 7.4). Alternatively, the mixture was reacidified after this back-neutralization step, liposomes were added and lipid mixing was recorded at pH 5.0 (pH 5.0/pH 7.4/pH 5.0). Control HCVpps were left at pH 7.4 throughout the fusion reaction with liposomes (pH 7.4).

fusion process (Lavillette *et al.*, 2006). For this purpose, we performed HCVpp lipid mixing assays using fluorescence spectroscopy and analysed two conditions: (i) HCVpp pre-exposed to pH 5.0 in the absence of liposomes; (ii) HCVpp pre-exposed to pH 5.0 in the absence of liposomes and back neutralized. The results are presented in Fig. 7. When HCVpps were pre-incubated at low pH in the absence of target membranes, their subsequent lipid mixing capacity with liposomes decreased as the incubation time at pH 5.0 increased (Fig. 7a). Although fusion activity was totally lost after a 10 min pre-incubation at pH 5.0, HCVpps retained, respectively, 50, 20 and 15 % of their fusion capacity after 30, 45 and 60 s of low-pH pre-incubation, indicating a relative resistance of HCVpps to low pH. This is in line with the hypothesis that HCV fusion protein(s) undergo a low pH-dependent conformational change. This behaviour must be compared with what has been reported previously for tick-borne encephalitis virus, a member, like HCV, of the family *Flaviviridae*. Indeed, virtually all fusion activity was lost after only 30 s of low-pH pre-incubation (Corver *et al.*, 2000). Our result with HCVpps compared with that of SFV and Sindbis virus fusion, where 90 % of their fusion capacity is lost after 35 and 60 s, respectively, at low pH in the absence of target membranes (Smit *et al.*, 1999; Waarts *et al.*, 2005). When HCVpps were pre-incubated at pH 5.0 for 1 min, followed by back neutralization in the absence of liposomes, lipid mixing resumed only when reacidification was performed (Fig. 7b, pH 5.0/pH 7.4/pH 5.0). Under these conditions, around 20 % of viral fusion activity could be restored. Without this reacidification step, no fluorescence dequenching was observed (Fig. 7b, pH 5.0/pH 7.4). This result extends our previous data (Lavillette *et al.*, 2006) and is in line with the results in Fig. 7(a), indicating a relative resistance of HCVpps and of their envelope glycoproteins to low-pH pre-treatment.

Membrane fusion of AIVpps with liposomes triggered at low pH

Our cryo-TEM observations of HCVpp revealed the early stages in their interaction with liposomes at low pH, but we could not observe a complete membrane merging. To test our hypothesis that, although measurable by fluorescence spectroscopy (Lavillette *et al.*, 2006), HCV-mediated fusion with liposomes is an event too scarce to be directly observed, we studied AIVpp interaction with liposomes containing a mixture of gangliosides known to act as receptors for AIV (Stegmann *et al.*, 1986, 1989). Under these conditions, HA-mediated fusion is known to be optimal, although measurable fusion could be observed in the absence of these lipids (Stegmann *et al.*, 1985).

As shown in Fig. 8, AIVpps were found in contact with liposomes at neutral pH, without any visible membrane deformation (Fig. 8a, b). Lowering the pH to 5.0 induced extensive conformational changes in HA that triggered membrane fusion. Indeed, HA proteins no longer displayed well-organized rod-like structures but instead adopted a dishevelled appearance (Fig. 8c, arrow), whilst the pseudoparticles adopted an irregular shape. In addition, liposomes interacting with AIVpps clearly underwent membrane deformations at the contact zone. Importantly, cryo-TEM images revealed large liposomes containing one viral capsid (Fig. 8d–f, asterisks) and showing disordered densities at their lipid surface corresponding to distorted HA proteins (Fig. 8, arrows). This clearly demonstrated that membrane fusion processes occurring between AIVpps and liposomes are triggered at low pH. During this process, the nucleocapsid remained intact (Fig. 8, asterisks), whilst distorted HA proteins were unevenly distributed on the liposome surface (Fig. 8, arrows). These findings clearly provided evidence of a pH-dependent membrane fusion process between pseudotyped particles and liposomes, observed at a nanometric resolution.

Our success in observing AIVpp-mediated fusion in the presence of gangliosides suggests the importance of a receptor present on the target membrane. Similarly, the cryo-TEM study of membrane fusion induced by HCV E1–E2 may require the use of specific ligands such as HCV receptors or parts of receptors grafted onto liposomes, which would help us to progress in our understanding of HCV fusion. In addition, the number of glycoproteins present on the surface of pseudotyped particles probably plays a key role in the formation of the fusion pore. From our present observations and from previous data indicating lower infectivity and fusogenicity for HCVpps compared with AIVpps (Lavillette *et al.*, 2006), the number of E1–E2 complexes on the surface of HCVpp is probably lower than that of HA on the surface of AIVpps (Sandrin & Cosset, 2006), which is not favourable for the direct observation of HCV fusion events. Further investigations are needed for a more thorough understanding of the underlying mechanism of HCV fusion.

In conclusion, our efficient method of virus particle sorting through the use of magnetic nanobeads is a direct approach easily adaptable to the extensive characterization of any virus by EM at a nanometer scale. This has allowed us to characterize HCVpps by cryo-TEM for the first time, as well as to observe some molecular details of the HCVpp–lipid membrane interaction involved in the pH-dependent fusion process. However, the characterization of HCV E1–E2 at the particle surface remained out of reach by our approach, most probably due to a combination of several features: the small size of both proteins, their high level of glycosylation, their possible flat orientation on the viral membrane and the presence of large, poorly structured regions in the ectodomain of E2.

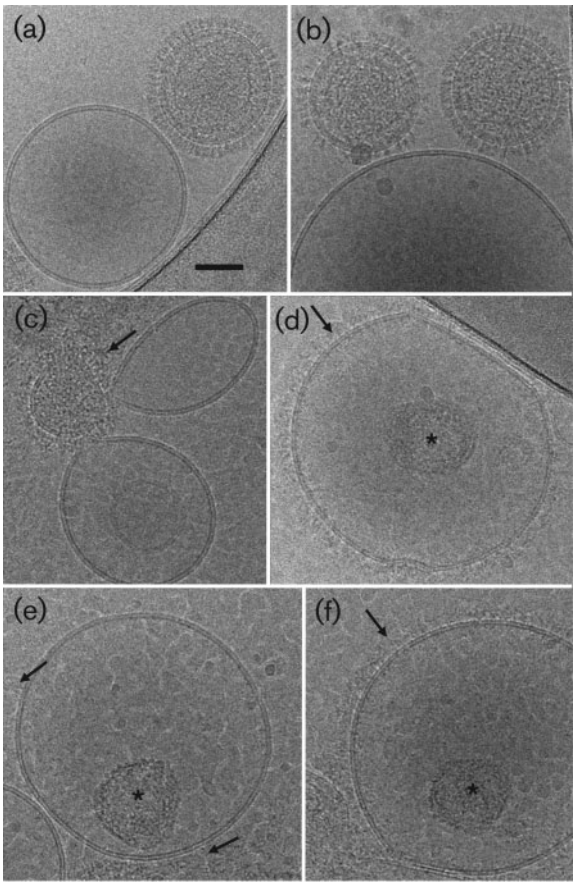

Fig. 8. Membrane fusion of AIVpps with liposomes at low pH. (a, b) AIVpps interacting at neutral pH with large unilamellar vesicles (LUVs) exposing gangliosides. (c–f) At pH 5, the early steps of membrane fusion are induced by HA conformational changes. HA changed its regular rod-like shape (a, b) into a distorted structure (black arrow), clearly visible on AIVpps involved in the fusion process with liposomes (c). Complete membrane fusion was observed, revealing intact nucleocapsids (black asterisks) within fused liposomes (d–f). Bar, 50 nm.

METHODS

Antibodies. Anti-HCV E1 mAb A4and E2 mAbs H48 and H53 (a kind gift from J. Dubuisson, Institut de Biologie de Lille, France) were

used for HCVpp immunosorting. The anti-SFV E1 polyclonal antibody was a kind gift from M. Sjöberg (Karolinska, Sweden). The polyclonal antibody against the H7 subtype of HA (anti-Kp-Ro Rostock cl96-11) was kindly provided by W. Garten (Marburg, Germany).

Preparation of liposomes. Large unilamellar vesicles (LUVs) were prepared from egg yolk phosphatidylcholine (PC) (Avanti Polar Lipids) and cholesterol (chol; Sigma-Aldrich) at a final concentration of 5 mM and a molar ratio of 70 : 30. Liposomes were prepared by extrusion through a stack of 100 nm pore size polycarbonate filters (device from Avestin) to obtain a homogeneous size, as described previously (Lavillette *et al.*, 2006). For liposome capture on streptavidin magnetic beads, 0.05 % biotin–PE was added to the lipid mixture, and liposomes were prepared by extrusions through a stack of 100 nm pore size polycarbonate filters. For observations of AIVpp membrane fusion, 200 nm LUVs contained dioleoyl phosphatidic acid (Avanti Polar Lipids), PC, chol and gangliosides (a mixture from bovine brain, estimated molar mass 1500 g mol^{-1}; Calbiochem) at a molar ratio of 0.5 : 5.5 : 3 : 1. For fluorescence spectroscopy measurements, 100 nm LUVs were composed of PC : chol : octadecyl rhodamine (R_{18}) at a molar ratio of 65 : 30 : 5.

Vector constructs and preparation of pseudoparticles. The cytomegalovirus (CMV)–Gag–Pol murine leukemia virus (MLV) packaging construct, encoding the MLV *gag* and *pol* genes, and the MLV–GFP plasmid, encoding a MLV-based transfer vector containing a CMV–GFP internal transcriptional unit, have been described previously (Bartosch *et al.*, 2003a). The phCMVHA (Hatziioannou *et al.*, 1998) and NA expression vectors encoded the HA and NA of AIV (fowl plague virus), respectively. The plasmid phCMV-E1E2-HCV (Bartosch *et al.*, 2003a) encoded the HCV E1 and E2 glycoproteins of genotype 1a, strain H77 (GenBank accession no. AF009606). The SFV expression vector encoded the SFV E3 to E1 glycoproteins (Kahl *et al.*, 2004). Pseudoparticles bearing the E1 and E2 envelope glycoproteins of HCV (HCVpp), the HA and NA of AIV (AIVpp) or the E1 and E2 envelope proteins of SFV (SFVpp) were then generated and purified as described previously (Bartosch *et al.*, 2003a; Lavillette *et al.*, 2006). Particles produced without any envelope expression construct were denoted NoEnvpps.

Conventional TEM and cryo-TEM. For immunogold labelling, pseudotyped particles deposited onto nickel/formvar grids were first incubated with fatty acid-free BSA in PBS (2 % final concentration), followed by incubation with an antibody directed against HCV E1 or E2 (mAb A4 or H53, respectively). After extensive washing, the grids were floated onto a drop of secondary antibody grafted to 10 nm colloidal gold particles, followed by fixation with 1 % glutaraldehyde and negative staining with 1 % uranyl acetate. Observation was performed at 80 kV with a Philips CM120 TEM microscope. For cryo-TEM, a 5 µl sample was deposited onto a holey carbon-coated copper grid; the excess was blotted with filter paper and the grid was plunged into a liquid ethane bath cooled with liquid nitrogen (Leica EM CPC). Specimens were maintained at a temperature of approximately –170 °C, using a cryo holder (Gatan) and observed with a FEI Tecnai F20 electron microscope operating at 200 kV and at a nominal magnification of 50 000 × under low-dose conditions. Images were recorded with a 2k × 2k low-scan CCD camera (Gatan).

Fusion assays by fluorescence spectroscopy. HCVpps were pre-exposed to pH 5.0 in a 37 °C thermostat-controlled 96-well plate in PBS in the absence of liposomes for the indicated time intervals. Lipid mixing was subsequently performed at pH 5.0 by adding liposomes to the wells. In another set of experiments, HCVpps were pre-exposed to pH 5.0 for 1 min in the absence of liposomes and then either the pH was returned to neutral and liposomes were added, or the pH was returned to neutral, liposomes were added and the fusion mixture was reacidified to pH 5.0. Lipid mixing between HCVpps and liposomes was monitored as the dequenching of R_{18}, as described previously (Lavillette *et al.*, 2006). Fusion kinetics were recorded on an Infinite 1000 TECAN fluorimeter over a 10 min time period, at $\lambda_{excitation}$=560 nm and $\lambda_{emission}$=590 nm. Maximal R_{18} dequenching was measured after the addition of Triton X-100 (0.1 % final concentration) to the wells.

Immunopurification of HCVpps and AIVpps using magnetic beads. Protein A- or protein G-conjugated superparamagnetic beads (Bio-Adembeads) were purchased from Ademtech. Before use, the beads were washed with a large volume of working buffer [145 mM NaCl, 1 mM EDTA, 2.5 mM HEPES (pH 7.4)]. The magnetic beads (5 µl) were incubated with H48 or H53 anti-HCV E2 mAb or a polyclonal antibody against the H7 subtype of HA, in a final volume of 100 µl, at 4 °C for 30 min. The magnetic bead–protein A/G–antibody complex was sedimented with a magnet. The pellet was washed three times to remove excess antibody. Beads coated with antibody were incubated with HCVpps or AIVpps at room temperature for 30 min (final volume 100 µl). After sedimentation with the magnet, the pellet was washed to remove unbound HCVpps or AIVpps. Cryo-TEM grids were then prepared with this suspension, without any further treatment. Semi-quantitative evaluation of the number of HCVpps immunocaptured by this strategy was performed after Western blotting. In brief, HCVpps were first immunocaptured using protein G beads as described above and washed extensively, and, after collection of the beads with the magnet, captured particles were detached from the beads with boiling Laëmmli buffer and their content in terms of MLV capsid and HCV E1 and E2 proteins was analysed by SDS-PAGE followed by Western blotting.

Immunolabelling of E2 onto immune-sorted HCVpps using protein A–colloidal gold solution. HCVpps were sorted using Bio-Adembeads and mAb H53. These immunosorted HCVpp were then further incubated with H53, and excess mAb was removed by washing and sedimentation using the above magnetic procedure. Protein A conjugated to 10 nm colloidal gold was added to detect mAb bound to the E2 glycoprotein exposed on HCVpps. After a 10 min incubation, excess gold particles were removed. The suspension was observed by cryo-TEM.

HCVpp membrane fusion observation by cryo-TEM. For this experiment, three procedures were performed. The first consisted of adding HCVpps to an LUV suspension in pH 5.0 buffer A (15 mM sodium citrate, 10 mM MES, 5 mM HEPES, 135 mM NaCl, 1 mM EDTA) at room temperature. In the second procedure, LUVs concentrated by ultracentrifugation (10 µl at 100 mM) were added to a pellet of HCVpps sorted with mAb H53–Bio-Adembeads at neutral pH. The pH was then lowered with 50 µl buffer A. After a 15 min incubation at room temperature, corresponding to the time needed to reach the plateau of membrane fusion kinetics described by Lavillette *et al.* (2006), unreacted liposomes were removed using the magnet purification step. This suspension was then observed by cryo-TEM. The third procedure consisted of preparing liposomes containing biotin–PE. Streptavidin-conjugated magnetic beads were then mixed with biotinylated liposomes and the resulting mixture was incubated with HCVpps at low pH and observed by cryo-TEM.

AIVpp membrane fusion observation by cryo-TEM. AIVpps were mixed for 10 min at room temperature with 200 nm LUVs (1 mM final concentration) suspended in neutral or pH 5.0 buffer and observed by cryo-TEM.

ACKNOWLEDGEMENTS

This work was supported by the CNRS and the 'Agence Nationale de Recherche pour le SIDA et les hépatites virales' (ANRS) (to O. L. and

E.-I. P). O. L. B. is the recipient of PhD fellowships from 'Vaincre la Mucoviscidose'. Jean Dubuisson is gratefully acknowledged for the kind gift of HCV anti-E1 and anti-E2 antibodies and plasmids for HCVpp production, and Olivier Diaz for the gift of magnetic columns and for helpful advice. Conventional TEM was performed at the Centre Technologique des Microstructures, Université Lyon 1, La Doua.

REFERENCES

Bartosch, B. & Cosset, F. L. (2006). Cell entry of hepatitis C virus. *Virology* **348**, 1–12.

Bartosch, B. & Cosset, F. L. (2009). Studying HCV cell entry using HCV pseudoparticles (HCVpp). *Methods Mol Biol* **510**, 279–293.

Bartosch, B., Dubuisson, J. & Cosset, F. L. (2003a). Infectious hepatitis C virus pseudo-particles containing functional E1–E2 envelope protein complexes. *J Exp Med* **197**, 633–642.

Bartosch, B., Vitelli, A., Granier, C., Goujon, C., Dubuisson, J., Pascale, S., Scarselli, E., Cortese, R., Nicosia, A. & Cosset, F. L. (2003b). Cell entry of hepatitis C virus requires a set of co-receptors that include the CD81 tetraspanin and the SR-B1 scavenger receptor. *J Biol Chem* **278**, 41624–41630.

Blanchard, E., Belouzard, S., Goueslain, L., Wakita, T., Dubuisson, J., Wychowski, C. & Rouille, Y. (2006). Hepatitis C virus entry depends on clathrin-mediated endocytosis. *J Virol* **80**, 6964–6972.

Chapel, C., Garcia, C., Bartosch, B., Roingeard, P., Zitzmann, N., Cosset, F. L., Dubuisson, J., Dwek, R. A., Trepo, C. & other authors (2007). Reduction of the infectivity of hepatitis C virus pseudoparticles by incorporation of misfolded glycoproteins induced by glucosidase inhibitors. *J Gen Virol* **88**, 1133–1143.

Corver, J., Ortiz, A., Allison, S. L., Schalich, J., Heinz, F. X. & Wilschut, J. (2000). Membrane fusion activity of tick-borne encephalitis virus and recombinant subviral particles in a liposomal model system. *Virology* **269**, 37–46.

Dreux, M., Pietschmann, T., Granier, C., Voisset, C., Ricard-Blum, S., Mangeot, P. E., Keck, Z., Foung, S., Vu-Dac, N. & other authors (2006). High density lipoprotein inhibits hepatitis C virus-neutralizing antibodies by stimulating cell entry via activation of the scavenger receptor BI. *J Biol Chem* **281**, 18285–18295.

Drummer, H. E., Maerz, A. & Poumbourios, P. (2003). Cell surface expression of functional hepatitis C virus E1 and E2 glycoproteins. *FEBS Lett* **546**, 385–390.

Dubochet, J., Adrian, M., Chang, J. J., Homo, J. C., Lepault, J., McDowall, A. W. & Schultz, P. (1988). Cryo-electron microscopy of vitrified specimens. *Q Rev Biophys* **21**, 129–228.

Fujiyoshi, Y., Kume, N. P., Sakata, K. & Sato, S. B. (1994). Fine structure of influenza A virus observed by electron cryo-microscopy. *EMBO J* **13**, 318–326.

Haid, S., Pietschmann, T. & Pecheur, E. I. (2009). Low pH-dependent hepatitis C virus membrane fusion depends on E2 integrity, target lipid composition, and density of virus particles. *J Biol Chem* **284**, 17657–17667.

Harris, A., Cardone, G., Winkler, D. C., Heymann, J. B., Brecher, M., White, J. M. & Steven, A. C. (2006). Influenza virus pleiomorphy characterized by cryoelectron tomography. *Proc Natl Acad Sci U S A* **103**, 19123–19127.

Hatziioannou, T., Valsesia-Wittmann, S., Russell, S. J. & Cosset, F. L. (1998). Incorporation of fowl plague virus hemagglutinin into murine leukemia virus particles and analysis of the infectivity of the pseudotyped retroviruses. *J Virol* **72**, 5313–5317.

Helle, F. & Dubuisson, J. (2008). Hepatitis C virus entry into host cells. *Cell Mol Life Sci* **65**, 100–112.

Helle, F., Goffard, A., Morel, V., Duverlie, G., McKeating, J., Keck, Z. Y., Foung, S., Penin, F., Dubuisson, J. & Voisset, C. (2007). The neutralizing activity of anti-hepatitis C virus antibodies is modulated by specific glycans on the E2 envelope protein. *J Virol* **81**, 8101–8111.

Hsu, M., Zhang, J., Flint, M., Logvinoff, C., Cheng-Mayer, C., Rice, C. M. & McKeating, J. A. (2003). Hepatitis C virus glycoproteins mediate pH-dependent cell entry of pseudotyped retroviral particles. *Proc Natl Acad Sci U S A* **100**, 7271–7276.

Kahl, C. A., Marsh, J., Fyffe, J., Sanders, D. A. & Cornetta, K. (2004). Human immunodeficiency virus type 1-derived lentivirus vectors pseudotyped with envelope glycoproteins derived from Ross River virus and Semliki Forest virus. *J Virol* **78**, 1421–1430.

Keck, Z. Y., Sung, V. M., Perkins, S., Rowe, J., Paul, S., Liang, T. J., Lai, M. M. & Foung, S. K. (2004). Human monoclonal antibody to hepatitis C virus E1 glycoprotein that blocks virus attachment and viral infectivity. *J Virol* **78**, 7257–7263.

Kielian, M. (2006). Class II virus membrane fusion proteins. *Virology* **344**, 38–47.

Kobayashi, M., Bennett, M. C., Bercot, T. & Singh, I. R. (2006). Functional analysis of hepatitis C virus envelope proteins, using a cell-cell fusion assay. *J Virol* **80**, 1817–1825.

Koutsoudakis, G., Kaul, A., Steinmann, E., Kallis, S., Lohmann, V., Pietschmann, T. & Bartenschlager, R. (2006). Characterization of the early steps of hepatitis C virus infection by using luciferase reporter viruses. *J Virol* **80**, 5308–5320.

Krey, T., d'Alayer, J., Kikuti, C. M., Saulnier, A., Damier-Piolle, L., Petitpas, I., Johansson, D. X., Tawar, R. G., Baron, B. & other authors (2010). The disulfide bonds in glycoprotein E2 of hepatitis C virus reveal the tertiary organization of the molecule. *PLoS Pathog* **6**, e1000762.

Lavillette, D., Bartosch, B., Nourrisson, D., Verney, G., Cosset, F. L., Penin, F. & Pécheur, E. I. (2006). Hepatitis C virus glycoproteins mediate low pH-dependent membrane fusion with liposomes. *J Biol Chem* **281**, 3909–3917.

Lavillette, D., Pécheur, E. I., Donot, P., Fresquet, J., Molle, J., Corbau, R., Dreux, M., Penin, F. & Cosset, F. L. (2007). Characterization of fusion determinants points to the involvement of three discrete regions of both E1 and E2 glycoproteins in the membrane fusion process of hepatitis C virus. *J Virol* **81**, 8752–8765.

Lindenbach, B. D. & Rice, C. M. (2001). *Flaviviridae*: the viruses and their replication. In *Fields Virology*, pp. 991–1041. Edited by D. M. Knipe & P. M. Howley. Philadelphia: Lippincott-Raven.

Lindenbach, B. D., Evans, M. J., Syder, A. J., Wolk, B., Tellinghuisen, T. L., Liu, C. C., Maruyama, T., Hynes, R. O., Burton, D. R. & other authors (2005). Complete replication of hepatitis C virus in cell culture. *Science* **309**, 623–626.

Mancini, E. J., Clarke, M., Gowen, B. E., Rutten, T. & Fuller, S. D. (2000). Cryo-electron microscopy reveals the functional organization of an enveloped virus, Semliki Forest virus. *Mol Cell* **5**, 255–266.

Moradpour, D., Penin, F. & Rice, C. M. (2007). Replication of hepatitis C virus. *Nat Rev Microbiol* **5**, 453–463.

Mukhopadhyay, S., Kim, B. S., Chipman, P. R., Rossmann, M. G. & Kuhn, R. J. (2003). Structure of West Nile virus. *Science* **302**, 248.

Mukhopadhyay, S., Kuhn, R. J. & Rossmann, M. G. (2005). A structural perspective of the flavivirus life cycle. *Nat Rev Microbiol* **3**, 13–22.

Op De Beeck, A., Cocquerel, L. & Dubuisson, J. (2001). Biogenesis of hepatitis C virus envelope glycoproteins. *J Gen Virol* **82**, 2589–2595.

Op De Beeck, A., Voisset, C., Bartosch, B., Ciczora, Y., Cocquerel, L., Keck, Z., Foung, S., Cosset, F. L. & Dubuisson, J. (2004). Characterization of functional hepatitis C virus envelope glycoproteins. *J Virol* **78**, 2994–3002.

Paredes, A. M., Brown, D. T., Rothnagel, R., Chiu, W., Schoepp, R. J., Johnston, R. E. & Prasad, B. V. (1993). Three-dimensional structure of a membrane-containing virus. *Proc Natl Acad Sci U S A* **90**, 9095–9099.

Sandrin, V. & Cosset, F. L. (2006). Intracellular versus cell surface assembly of retroviral pseudotypes is determined by the cellular localization of the viral glycoprotein, its capacity to interact with Gag, and the expression of the Nef protein. *J Biol Chem* **281**, 528–542.

Smit, J. M., Bittman, R. & Wilschut, J. (1999). Low-pH-dependent fusion of Sindbis virus with receptor-free cholesterol- and sphingolipid-containing liposomes. *J Virol* **73**, 8476–8484.

Stegmann, T., Hoekstra, D., Scherphof, G. & Wilschut, J. (1985). Kinetics of pH-dependent fusion between influenza virus and liposomes. *Biochemistry* **24**, 3107–3113.

Stegmann, T., Hoekstra, D., Scherphof, G. & Wilschut, J. (1986). Fusion activity of influenza virus. A comparison between biological and artificial target membrane vesicles. *J Biol Chem* **261**, 10966–10969.

Stegmann, T., Nir, S. & Wilschut, J. (1989). Membrane fusion activity of influenza virus. Effects of gangliosides and negatively charged phospholipids in target liposomes. *Biochemistry* **28**, 1698–1704.

Strauss, J. H. & Strauss, E. G. (2001). Virus evolution: how does an enveloped virus make a regular structure? *Cell* **105**, 5–8.

Tscherne, D. M., Jones, C. T., Evans, M. J., Lindenbach, B. D., McKeating, J. A. & Rice, C. M. (2006). Time- and temperature-dependent activation of hepatitis C virus for low-pH-triggered entry. *J Virol* **80**, 1734–1741.

Waarts, B. L., Smit, J. M., Aneke, O. J., McInerney, G. M., Liljestrom, P., Bittman, R. & Wilschut, J. (2005). Reversible acid-induced inactivation of the membrane fusion protein of Semliki Forest virus. *J Virol* **79**, 7942–7948.

Wakita, T., Pietschmann, T., Kato, T., Date, T., Miyamoto, M., Zhao, Z., Murthy, K., Habermann, A., Krausslich, H. G. & other authors (2005). Production of infectious hepatitis C virus in tissue culture from a cloned viral genome. *Nat Med* **11**, 791–796.

Yu, X., Qiao, M., Atanasov, I., Hu, Z., Kato, T., Liang, T. & Zhou, Z. (2007). Cryo-electron microscopy and three-dimensional reconstructions of hepatitis C virus particles. *Virology* **367**, 126–134.

Zhang, W., Chipman, P. R., Corver, J., Johnson, P. R., Zhang, Y., Mukhopadhyay, S., Baker, T. S., Strauss, J. H., Rossmann, M. G. & Kuhn, R. J. (2003). Visualization of membrane protein domains by cryo-electron microscopy of dengue virus. *Nat Struct Biol* **10**, 907–912.

Zhong, J., Gastaminza, P., Cheng, G., Kapadia, S., Kato, T., Burton, D. R., Wieland, S. F., Uprichard, S. L., Wakita, T. & Chisari, F. V. (2005). Robust hepatitis C virus infection *in vitro*. *Proc Natl Acad Sci U S A* **102**, 9294–9299.

Zhu, P., Liu, J., Bess, J., Jr, Chertova, E., Lifson, J. D., Grise, H., Ofek, G. A., Taylor, K. A. & Roux, K. H. (2006). Distribution and three-dimensional structure of AIDS virus envelope spikes. *Nature* **441**, 847–852.